RESEARCH ARTICLE | JANUARY 24 2024

Wind turbine wake superposition under pressure gradient

Arslan Salim Dar ; Fernando Porté-Agel

Physics of Fluids 36, 015145 (2024)
https://doi.org/10.1063/5.0185542

Physics of Fluids ARTICLE pubs.aip.org/aip/pof

Wind turbine wake superposition under pressure gradient

Cite as: Phys. Fluids **36**, 015145 (2024); doi: 10.1063/5.0185542
Submitted: 31 October 2023 · Accepted: 27 December 2023 ·
Published Online: 24 January 2024

Arslan Salim Dar and Fernando Porté-Agel[a)]

AFFILIATIONS

Wind Engineering and Renewable Energy Laboratory (WIRE), École Polytechnique Fédérale de Lausanne (EPFL), Lausanne 1015, Switzerland

[a)]Author to whom correspondence should be addressed: fernando.porte-agel@epfl.ch

ABSTRACT

We investigate the effect of pressure gradient on the cumulative wake of multiple turbines in wind tunnel experiments spanning across a range of adverse pressure gradient (APG), zero pressure gradient (ZPG), and favorable pressure gradient (FPG). Compared to the upstream-most turbine, the in-wake turbines exhibit lower (higher) wake velocity in APG (FPG) than in the ZPG. The maximum velocity deficit shows a lesser difference for the in-wake turbine between different cases compared to the upstream-most one. This is linked to the effect of the wake of the upstream turbine. Conversely, the wake width varies more for the in-wake turbines. A new analytical approach to model the cumulative wake velocity deficit is proposed. This approach extends the application of the analytical pressure gradient model to multiple turbine wakes. Specifically, the new approach explicitly accounts for the effect of the pressure gradient induced by the wake of the upstream turbine on the wake of the downstream one. The new method is compared to the linear summation approach and experimental data. It agrees well with the experiments and outperforms the linear summation approach.

I. INTRODUCTION

Onshore wind energy constitutes about 93% of the installed global wind energy capacity.[1] The continuous decrease in the levelized cost of electricity (LCOE) of onshore wind projects[2] and a push toward renewable energy sources have resulted in the rapid growth of onshore wind energy. Wind turbines are often installed in clusters, known as wind farms, where depending on the wind farm layout and wind direction, certain wind turbines operate in the wake of others. Turbine wakes, marked by lower velocity and higher turbulence, compared to the undisturbed flow, are responsible for lower available power and higher fluctuating loads on the in-wake turbines. While most of the existing literature on wind turbine wakes assumes a flat terrain,[3,4] wind turbines are often sited on non-flat topography in onshore conditions.

Flow over topography is inherently complex and depends significantly on the changes in surface elevation and roughness. The interaction of wind turbine wakes with the flow in complex terrain has been investigated in several wind tunnel,[5–8] numerical,[9–13] and field[14–16] studies. These studies have shown that the turbine power performance and wake characteristics such as its recovery, trajectory, expansion, and turbulence quantities are significantly affected by the flow in complex terrain.

One key feature of the flow in topography is the streamwise variation in velocity, which imposes a pressure gradient on the flow. The effect of pressure gradient on the development of planar wakes has been explored in several studies.[17–21] These studies showed that a pressure gradient can affect the recovery of the mean wake center velocity, where an adverse pressure gradient (APG) tends to slow it down and a favorable pressure gradient (FPG) tends to speed it up compared to a zero pressure gradient (ZPG) situation. In addition, the expansion of the wake in the cross-stream direction is also affected by the pressure gradient, with a higher wake width under an APG and a lower wake width under an FPG compared to that under a ZPG. The mean wake velocity deficit profiles were shown to be self-similar under pressure gradient situations, and the turbulence quantities were comparatively less affected by the pressure gradient.

The effect of pressure gradient imposed by the flow on wind turbine wakes has been recently investigated in several studies. Shamsoddin and Porté-Agel[22] proposed an analytical model for the far wake of a wind turbine under an imposed pressure gradient. In addition, they simulated a wind turbine wake using large-eddy simulation (LES) and extended some of the findings of planar wakes under pressure gradient to the axisymmetric ones. Shamsoddin and Porté-Agel[23] also performed a combined LES and analytical study of the wind turbine wake flow over a two-dimensional hill. They used their analytical model[22] together with the model of Hunt *et al.*[24] to model the wake of a wind turbine sited upstream of a hill with moderate slope. The LES results were used to validate the analytical framework. Using the LES, they also simulated several turbine positions across the hill and divided the flow over the hill into two regions of faster and slower wake recovery rates compared to a turbine in a flat terrain. They associated this behavior with the pressure gradient experienced by the turbine wake. Cai *et al.*[25] conducted wind tunnel experiments to investigate the effect of pressure gradient imposed by linear ramps on the turbine wake and power production. They also validated the model of Shamsoddin and Porté-Agel[22] with their experimental data. Dar *et al.*[26] performed a systematic study of wind turbines exposed to pressure gradient imposed by a flow linearly speeding up/slowing down from its induction region to the far wake. They showed that the wake deficit varies systematically with the change in pressure gradient, and the near wake length and the wake growth rate showed a linear relationship with the pressure gradient. They also showed that compared to ZPG, the power coefficient of the turbine increased with the increase in the FPG, whereas it decreased with the increase in the APG. More recently, Siguenza-Alvarado *et al.*[27] performed wind tunnel experiments of the wake of two aligned wind turbines on a two-dimensional hill. They showed that the advection terms play a key role in the wake recovery for steep hills.

As wind turbine wakes can lead to significant power losses in a wind farm (especially when the turbines in a row are fully aligned), it is of great interest to estimate these wake losses during the planning and the layout optimization phase of a wind farm. For this purpose, simplified engineering wake models are extremely popular, as they offer reasonably accurate and computationally inexpensive estimation of the mean wake velocity behind turbines. There are two categories: models for stand-alone wind turbine wakes and models that superpose multiple wakes to provide the estimation of the cumulative wake velocity behind a row of turbines. For stand-alone wind turbine wakes, several models have been proposed to estimate the mean wake velocity deficit in flat[28–34] and complex[22,26,35–37] terrains. As for the wake superposition models, several strategies have been proposed in the literature. The most popular of these are the linear summation principle[38,39] and the sum of squares approach.[40,41] These superposition models are, however, for the most part empirical, and more recently, some physics-based approaches have been proposed by Zong and Porté-Agel[42] and Bastankhah *et al.*[43] Although these superposition methods are designed for wind farms in flat terrain, they have been applied for wake superposition in complex terrain as well (see, e.g., Refs. 35 and 36). Lanzilao and Meyers[44] also proposed a wake superposition method for a varying base flow velocity field with application to offshore wind farms close to coastlines.

In this work, we perform a combined experimental and analytical study of multiple wind turbines exposed to a base flow pressure gradient. As the existing literature isolating the effect of pressure gradient on wind turbine wakes focuses on single turbine cases, we look to provide useful physical insights into the case of multiple turbine wakes exposed to a quasi-linear surrounding base flow. In addition, we propose two different strategies of modeling the cumulative wake behind multiple turbines in flat, as well as, complex terrain. The first approach is a modified version of the linear sum approach proposed by Niyaifar and Porté-Agel[39] adapted for streamwise variation in the base flow. The second approach is to use the pressure gradient model,[22,26] which accounts for the effect of the upstream turbine(s) in the base flow term. This approach eliminates the need for any subsequent superposition method to combine stand-alone wakes of the turbines and can model the cumulative wakes, both in flat and complex terrain. The rest of the article is organized as follows: Sec. II presents a description of the experimental setup and results from the experiments; Sec. III details the modeling approaches and compares them; and Sec. IV provides a summary of the work and some concluding remarks.

II. EXPERIMENTS

A. Setup

The measurements are carried out in the boundary layer wind tunnel facility of École Polytechnique Fédérale de Lausanne (EPFL). The wind tunnel is a closed-loop type with a test section of dimensions $28 \times 2.56 \times 2$ m^3 (length $\times$ width $\times$ height), and a contraction with an area ratio of 5:1 is present at the inlet of the test section. The flow is conditioned through a series of honeycomb meshes and screens before the contraction. This ensures a low free-stream turbulence intensity ($< 1\%$) and a uniform flow at the inlet of the test section. The flow in the wind tunnel is driven by a 130 kW fan, which is capable of generating wind speeds up to 25 ms^{-1} in the test section.

A three-bladed horizontal axis miniature wind turbine with a rotor diameter D of 10.5 cm and a hub height z_h of 8.75 cm is used in this work. The turbine rotor is a scaled-down version of the WiRE-01 turbine,[45] where a scaling of 1:1.43 is kept between the original and the scaled-down rotor models. The power and thrust characteristics of the scaled-down turbine are characterized by Dar *et al.*,[46] which showed that the turbine performance is unaffected by scaling it down as long as the Reynolds number is comparable between the original and the scaled-down models. The rotor is 3D printed using a liquid photopolymer resin and is mounted on a direct current (DC) motor manufactured by Maxon Motors (model: DCX10L). The DC motor is connected to a servo controller in order to acquire data and control the operation of the turbine. For all the experiments, turbines are operated at the tip speed ratio corresponding to maximum power extraction. The power extracted by the turbine P is quantified by multiplying the shaft torque Q of the turbine by its rotational speed Ω. A frictional toque Q_f is added to the torque estimated by multiplying the generated current I with the torque constant K in order to estimate the total shaft torque. The details of the power measurement procedure are given in Bastankhah and Porté-Agel.[45]

Seven different pressure gradient situations are tested in this study, including one ZPG case corresponding to flat terrain. For non-zero pressure gradients, linear ramps are used to generate terrain-induced pressure gradients. The ramps used in this study are the same as the ones used by Dar *et al.*[26] The ramps are 13 rotor diameters long, and their height h is varied to change the slope. Three different ramp angles are used, corresponding to 13.1°, 8.8°, and 4.4°, where a positive slope leads to an FPG and a negative one induces an APG. The cases are labeled as "ZPG" for the zero pressure gradient one, "APG-I," "APG-II," and "APG-III" for APG cases with 4.4°, 8.8°, and 13.1° angles, respectively, and "FPG-I," "FPG-II," and "FPG-III" for FPG cases with 4.4°, 8.8°, and 13.1° angles, respectively. In the ZPG case, three wind turbines are placed in a fully aligned configuration, with an inter-turbine spacing of five rotor diameters. In the FPG and APG cases, however, two turbines are placed on the ramp with a spacing of five rotor diameters. This is due to the limitation of the ramp length, which can only allow for two turbines to be placed. The first turbine is placed three rotor diameters from the upstream edge of the ramp. This is done to ensure that the base flow (flow without the turbine) experienced by the turbine is unaffected by the ramp edge. The choice of ramps is made in order to generate a quasi-linear base flow increase or decrease with the streamwise distance under different pressure gradient situations. The turbines are placed such that their axis of rotation is parallel to the ramp surface. As the turbine motor has a current limitation for optimal operation, the inflow velocity is adjusted between different cases such that all turbines can be controlled at their optimal tip speed ratio.

Velocity measurements are performed using a two-dimensional two-component (2D2C) particle-image velocimetry (PIV) setup also known as a planar PIV setup. The measurements are performed in a vertical plane normal to the rotor plane and passing through the turbine centerline. The flow without any turbines, termed the base flow, and the flow with the turbines, termed the wake flow, are captured in the current study. The PIV system used in the study comprises a sCMOS (scientific Complementary Metal–Oxide–Semiconductor) camera (2560×2160 pixels) with a 50 mm lens, a dual pulse Nd:YAG laser (model: Litron lasers, Nano TRL 425-10), and a programable timing unit (model: LaVision, PTU-v9). The size of the field-of-view (FOV) is $6D \times 5D$, with a spatial resolution of 0.0189D, with an overlap of approximately 1D in the x direction between consecutive FOVs. The image pairs are captured at a sampling rate of 10 Hz, and 1000 instantaneous flow fields are used to obtain time-averaged flow statistics. Olive oil droplets of diameter on the order of several micrometers are used as seeding particles for flow measurements. Figure 1 shows a schematic of the experimental setup.

Image processing is performed using the DaVis software developed by LaVision. Reducing size interrogation windows of 64×64 pixels and 32×32 pixels is used for image cross correlation. An overlap of 75% is kept between consecutive windows, and the correlation is obtained after two passes through each window size. Bad velocity vectors are removed from the data using a universal outlier detection method and replaced using interpolation based on surrounding vectors. The maximum uncertainty in the mean velocity is estimated using the correlation statistics approach,[47] which gives a value of 0.06 ms^{-1} in the regions of high flow shear.

The floor of the tunnel is covered by double-rolled chains with an inter-chain spacing of 40 cm. In addition, a picket fence of dimensions 10 cm in length and 5 cm in height with spikes of 3 cm in length is placed at the inlet of the test section. This is done to facilitate the growth of a turbulent boundary layer (TBL) in the tunnel. Figure 2 characterizes the incoming turbulent boundary layer using the 2D2C PIV setup described above. The hub height velocity U_h is used for normalization with a high gradient in the normalized averaged streamwise velocity close to the wall. The boundary layer height is more than five rotor diameters and is similar to the one developed in Dar *et al.*[26] The streamwise turbulence intensity $I_u = \sigma_U / U_h$, where σ_U is the standard deviation in the streamwsie velocity, shows an almost linear decrease with height. The streamwise turbulence intensity at the hub height of a prospective turbine is 0.135. A logarithmic fit is performed on the velocity data in the surface layer ($\approx$ 20% of the boundary layer height). The result of the fit is shown in Fig. 2(b). The aerodynamic surface roughness z_0 and the friction velocity u_* are found to be 0.24 mm and 0.44 ms^{-1}, respectively. It is to be noted that the height coordinate z in Fig. 2 is set on the tunnel floor, while it is set on the first turbine hub position in the rest of the article.

The Reynolds number based on the hub height velocity at the location of the first turbine and the rotor diameter ranges between 44 000 and 49 000 for all the cases except the APG-III case, for which it is 57 000. Although the Reynolds number in the study is less than the utility-scale wind turbines, it is close to the threshold observed by Chamorro *et al.*[48] around which the mean flow characteristics become independent of the Reynolds number. In addition, it is well established

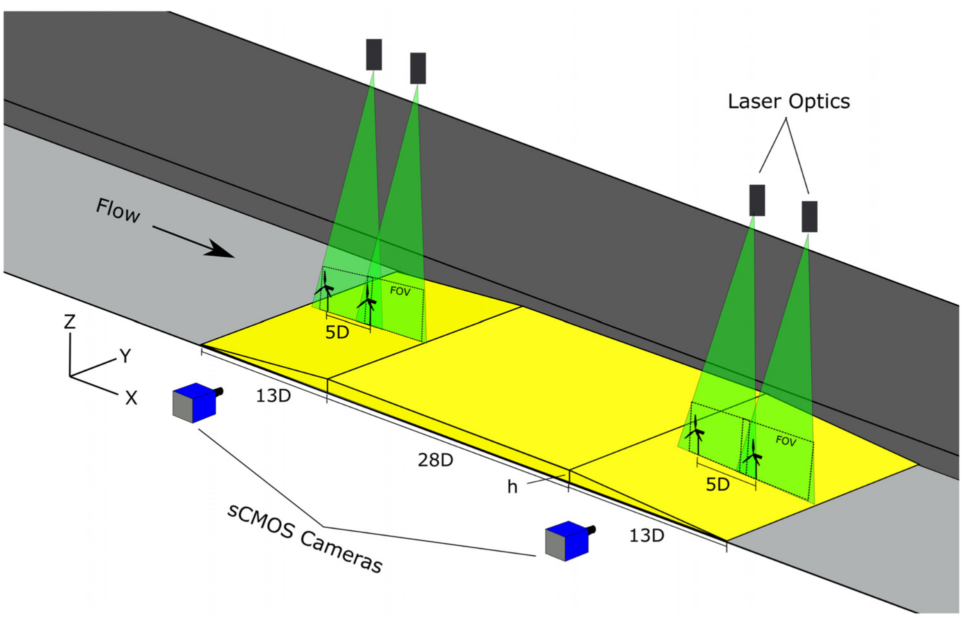

FIG. 1. Schematic of the experimental setup (not to scale). The shaded green rectangles marked by dashed black lines show the particle-image velocimetry field-of-views.

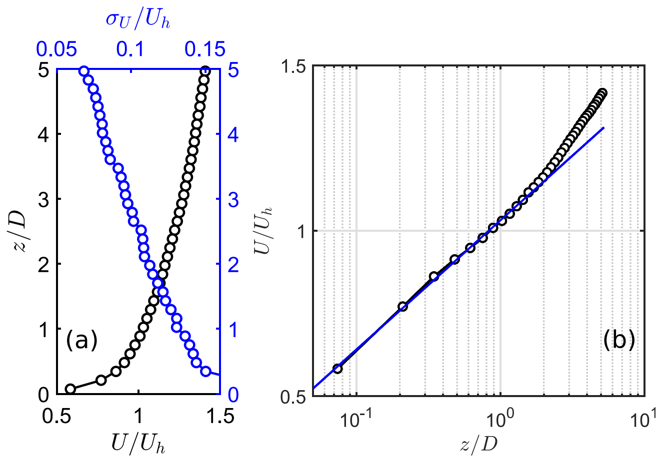

FIG. 2. Vertical profiles of the normalized averaged streamwise velocity and the streamwise turbulence intensity (a) and the normalized averaged streamwise velocity with the height coordinate in log scale (b). The lines with markers show the experimental data, and the solid blue line in (b) represents the logarithmic fit.

in the literature that the far-wake characteristics of wind turbines depend on the thrust coefficient. The miniature turbine used in the current study has a thrust coefficient comparable to the utility-scale ones.[46] In addition, the analytical modeling framework developed in this work is also dependent on the thrust coefficient and does not have any Reynolds number dependence. Therefore, the results of this study can provide useful insights for utility-scale turbines as well.

B. Results

Here, we present the results from the wind tunnel experiments. The results are sub-divided into two categories: we first report the results related to the flow without any turbines, which is followed by the results related to the turbine wake flow. For mean flow statistics, we define the mean streamwise velocity as $U = \sqrt{U_x^2 + U_z^2}$, where U_x and U_z are the mean horizontal and the vertical velocity components, respectively. It is to be noted that $(x, z) = (0, 0)$ represents the hub location of the first turbine in each case.

1. Base flow

Figure 3 shows the base flow contours of the normalized averaged streamwise velocity, together with the streamlines of the in-plane velocity vector field. The flow is homogeneous in the streamwise direction for the ZPG case but shows an acceleration and deceleration for the FPG and APG cases, respectively. The flow acceleration/deceleration increases with the increase in the ramp angle for the pressure gradient situations. The flow streamlines are approximately parallel to the surface for the ZPG and smallest ramp angles (APG-I and FPG-I), whereas they move away from the surface in the APG situation and move toward it in the FPG situation, with the increase in the ramp angle.

Figure 4(a) shows the normalized averaged streamwise velocity along the streamline originating from the hub position of a prospective turbine and along the local hub height for different pressure gradient situations. For most of the cases, the two velocities are comparable.

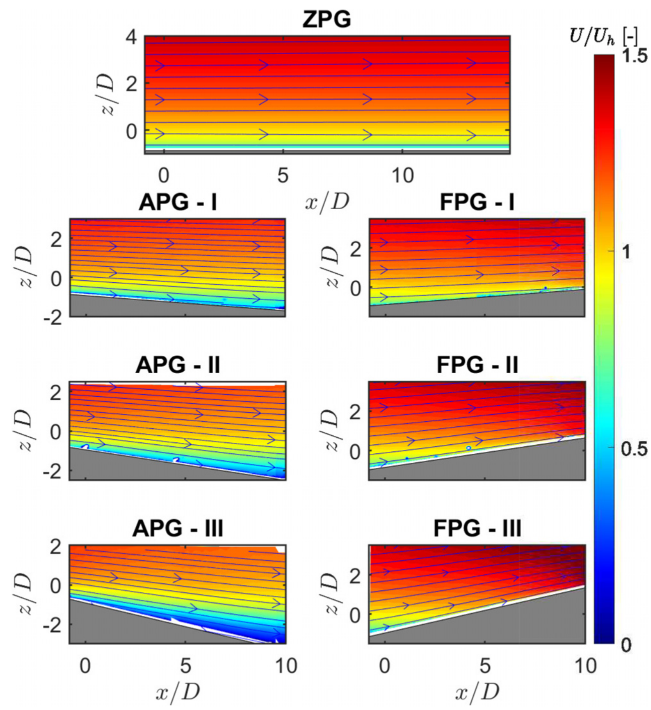

FIG. 3. Contours of the normalized averaged streamwise velocity in the base flow. The streamlines of the in-plane velocity vectors are overlaid on the contours.

However, the difference between them is significant for the APG-III case. This shows that the deviation of the flow streamlines from the ramp slope is marginal for the majority of the cases. For the APG-III case, the streamlines move away from the surface into a higher velocity flow, which causes an increase in the velocity compared to that at the local hub height. It can also be observed that the increase or decrease in velocity with the increase in the streamwise distance is approximately linear for all the cases, with the speed-up or slow down in velocity increasing with increasing ramp slope.

Following previous works (Refs. 21, 22, and 46), the streamwise pressure gradient is approximated by UdU/dx. A zero pressure gradient corresponds to $UdU/dx = 0$, a favorable pressure gradient corresponds to $UdU/dx > 0$, and an adverse pressure gradient corresponds to $UdU/dx < 0$. Figure 4(b) shows the normalized averaged pressure gradient along the velocity profiles shown in Fig. 4(a). For the favorable pressure gradient cases, a clear increase in the pressure gradient with the increase in the ramp angle can be observed for both velocities, i.e., the one along the streamline and the one along the local hub height. For the adverse pressure gradient cases, a clear increase in the pressure gradient can be observed for the velocity along the local hub height; however, the values get closer for the velocity along the streamline. The development of a shear layer along the ramp length in the adverse pressure gradient cases causes the streamlines to move away from the surface. As the shear layer is stronger in the APG-III case compared to the APG-II case, the deflection of the streamline is also larger, which leads to a decrease in the pressure gradient compared to that along the local hub height. As shown previously by Dar *et al.*,[26] a stand-alone wind turbine wake follows the base flow streamline

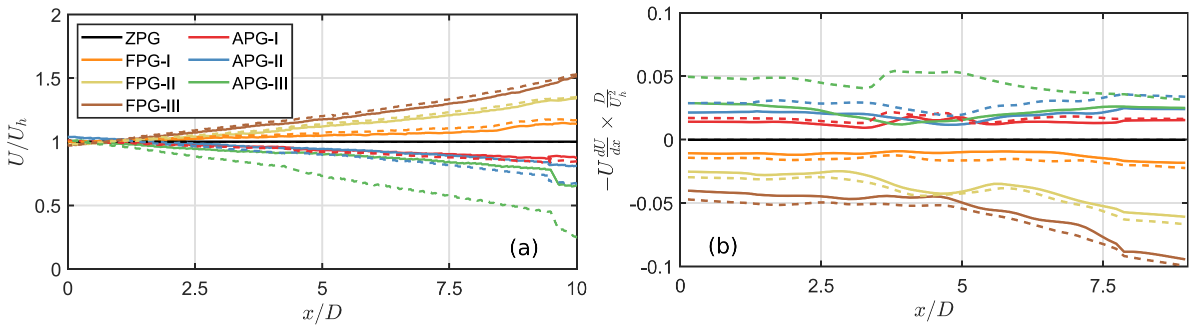

FIG. 4. Normalized averaged streamwise velocity (a) and the normalized pressure gradient (b) in the base flow along the streamline originating at $(x, z) = (0, 0)$ (solid lines) and along the local hub height (dashed lines) for different pressure gradient situations.

originating from the virtual hub height position; therefore, the velocity and pressure gradient profiles along the base flow streamline are more relevant for characterizing the wake flow.

The contours of the turbulence intensity based on the horizontal component of the velocity are shown in Fig. 5. High levels of turbulence intensity close to the surface are observed in the ZPG case. For the pressure gradient cases, the turbulence intensity also shows a significant change with the streamwise distance. For the APG cases, the turbulence intensity close to the surface increases with the streamwise distance from the ramp edge. Due to the negative slope of the ramp, the flow close to the surface of the ramp is sheltered from the upstream flow, which creates a shear layer with a high mean velocity gradient, and thereby, high turbulence intensity. For the FPG cases, on the other hand, the turbulence intensity close to the surface is observed to decrease with the increase in the streamwise distance. This can be related to the decrease in the mean flow shear close to the surface as the flow speeds up on the ramp. Figure 6 shows the turbulence intensity along the hub streamline in the base flow and the local hub height for all the cases. For all the cases, the turbulence intensity ranges between 0.12 and 0.155 along the streamline, with values increasing with distance for the APG cases and decreasing for the FPG cases.

The vertical momentum flux along with the mean flow shear is responsible for the production of turbulence in turbulent boundary layers. The vertical momentum flux can be associated with the coherent motions that are responsible for energy transfer from the mean flow to the turbulent flow.[49] Figure 7 shows the contours of the normalized averaged vertical momentum flux in the base flow for all the cases. The normalized averaged momentum flux shows the highest magnitude in the APG cases in the shear layer, which corresponds to high turbulence intensity. For the FPG cases, the magnitude of the normalized averaged momentum flux is lower than for the APG ones, and it is distributed over a larger vertical extent. In general, the trends in the normalized averaged vertical momentum flux are consistent with those in the turbulence intensity.

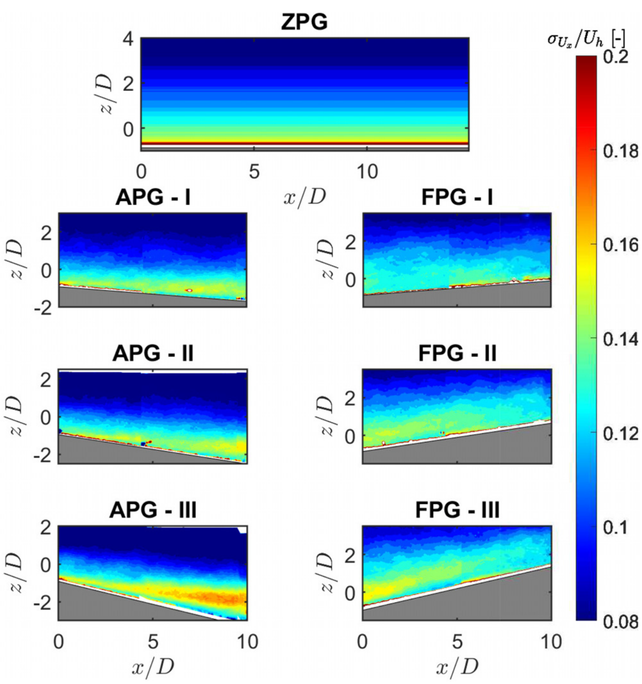

FIG. 5. Contours of the horizontal turbulence intensity in the base flow.

2. Wake flow

In this section, we present results related to the wake of multiple fully aligned wind turbines (3 in the case of ZPG and 2 in the pressure

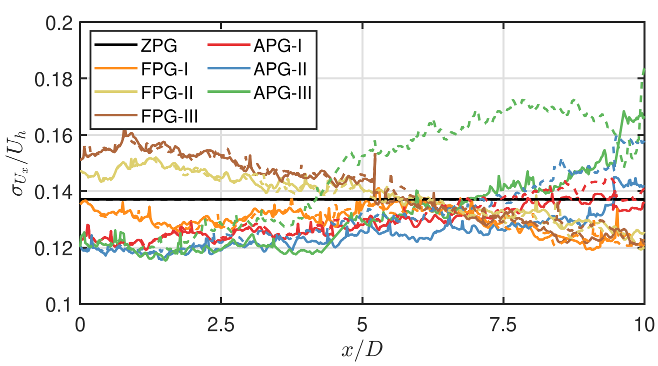

FIG. 6. Horizontal turbulence intensity in the base flow along the streamline originating at $(x, z) = (0, 0)$ (solid lines) and along the local hub height (dashed lines) for different pressure gradient situations.

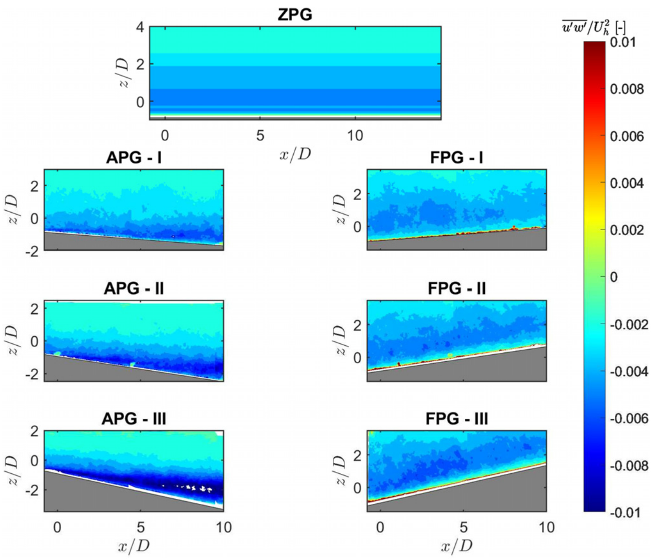

FIG. 7. Contours of the normalized averaged vertical momentum flux in the base flow.

gradient cases). Figure 8 shows the contours of the normalized averaged streamwise velocity in the wake flow for different pressure gradient situations. Previous studies Refs. 22, 25, and 26 have focused on stand-alone turbine wakes under the base flow pressure gradient. Here, we can observe that the normalized averaged streamwise velocity behind the second turbine is also affected by the ramp angle. In general, it is observed that the mean wake velocity decreases with the increase in the APG and increases with the increase in FPG, compared to the ZPG case, which is consistent with the previous studies Refs. 22, 25, and 26. For the ZPG case, the in-wake turbines have a lower velocity close to the turbine but a higher velocity further downstream compared to the turbine in the free flow. This is due to the turbine-added turbulence intensity, which enhances the wake recovery. For the APG-I case, a similar observation to the ZPG case is made. For the APG-II and APG-III cases, however, the wake velocity is observed to be lower for the second turbine compared to the first one. This can be related to the lower velocity in the base flow for the second turbine. For the FPG cases, an opposite trend is observed where the second turbine shows a higher wake velocity compared to the first turbine due to an increase in the base flow velocity with the increase in the streamwise distance. The horizontal turbulence intensity in the wake flow is shown in Fig. 9. A peak of turbulence intensity behind the rotor top tip can be seen in all the cases, which is associated with the high mean flow shear around that region.[50] For the ZPG case, the turbulence intensity increases behind the second and the third turbines compared to that behind the first one. This is associated with the turbulence intensity added by the upstream turbine(s). For the FPG cases, a higher turbulence intensity is observed compared to the ZPG one, which increases with the increase in the FPG, and in the wake of the second turbine compared to the first one. For the APG cases, on the other hand, the peak of the turbulence intensity is lower than the FPG cases, and there seems to be no significant increase in the turbulence intensity behind the second turbine compared to the first one. As can be seen in Fig. 9, for the FPG cases, the peak region of turbulence intensity behind the two turbines is approximately aligned, resulting in an overall increase in the turbulence intensity behind the second one. In the APG cases, as the wake moves away from the surface, the peak regions behind the two turbines are not completely aligned, which results in a turbulence

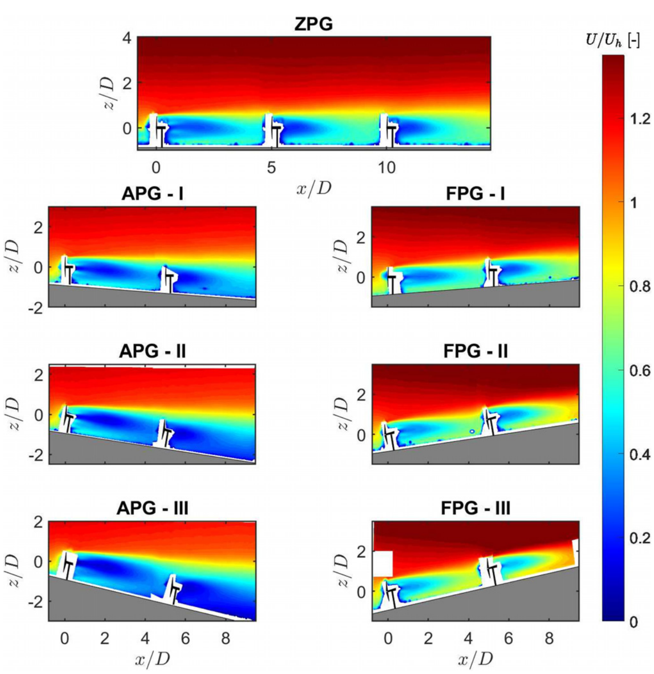

FIG. 8. Contours of the normalized averaged streamwise velocity in the wake flow.

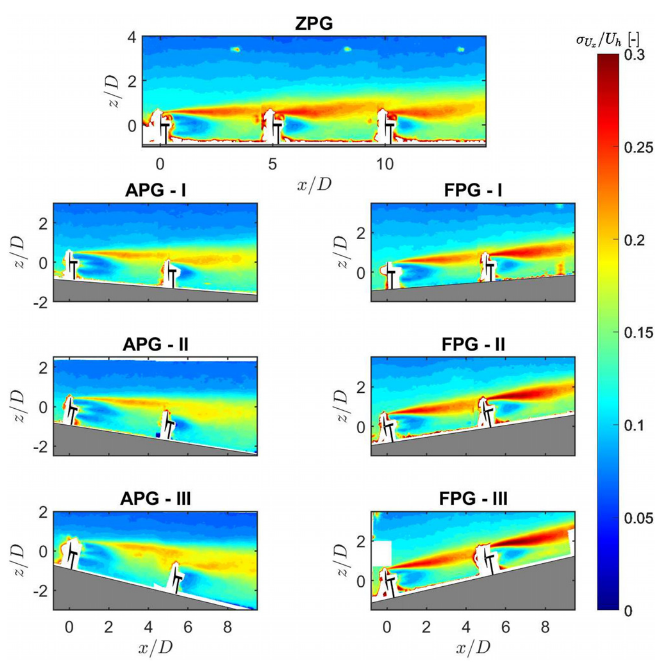

FIG. 9. Contours of the horizontal turbulence intensity in the wake flow.

intensity distribution downstream of the second turbine, with a peak value similar to that behind the first turbine and a larger vertical spread compared to the FPG cases.

Vertical momentum flux acts as a mechanism to re-energize the wake by bringing high momentum flow from the outside into the wake. The inclination of the terrain also has an effect on the vertical momentum flux in the wake flow. Figure 10 shows the contours of the normalized averaged vertical momentum flux in the wake for different cases. For the ZPG case, the normalized averaged vertical momentum flux shows a negative value around the upper wake edge and a positive value around the lower wake edge, indicating the entrainment of energy from above and below into the wake. For the APG cases, the negative region behind the rotor top tip grows stronger in magnitude and shows a high expansion in the vertical direction, similar to the expansion of the horizontal turbulence intensity profile. This is consistent with the expansion of the wake velocity profiles, which in the APG cases have a larger width.[26] The magnitude of the normalized averaged vertical momentum flux gets stronger with the increase in the ramp angle. For the FPG cases, the negative region of the vertical momentum flux behind the rotor top tip is smaller compared to the ZPG and APG cases, whereas the positive region behind the rotor bottom tip gets larger with the increase in the positive ramp angle. This indicates that the ramp inclination has an influence on the distribution of the momentum flux in the wake.

We now focus on characterizing the wake velocity deficit behind the turbines for different ramp cases. Here, the streamwise velocity deficit ΔU is defined as the difference between the base and wake flow velocities such that $\Delta U(x, z) = U_b(x, z) - U_w(x, z)$, where U_b and U_w are the base and the wake flow velocities, respectively. The mean wake trajectories identified by the position of the maximum averaged wake velocity deficit are also shown. Following Shamsoddin and Porté-Agel,[23] we plot contours of the averaged streamwise velocity deficit normalized by the base flow velocity at the hub position of the first

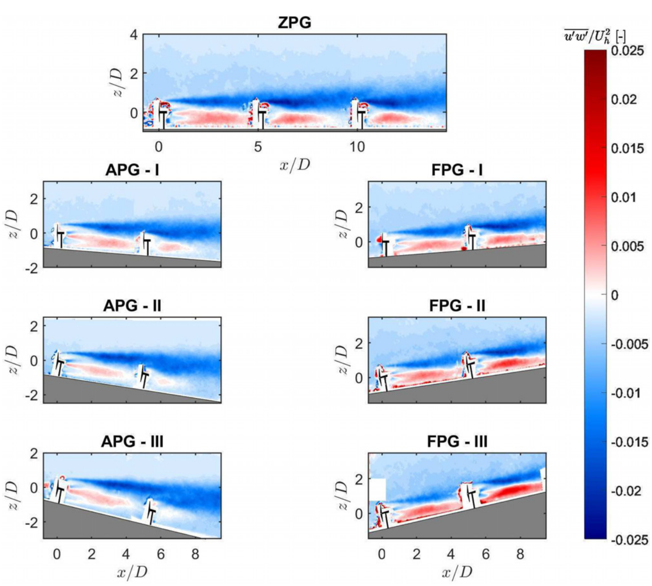

FIG. 10. Contours of the normalized averaged vertical momentum flux in the wake flow.

turbine [Fig. 11(a)] and normalized by the base flow velocity along the wake trajectory [Fig. 11(b)]. Following previous studies,[23,51] the wake trajectory is identified as the vertical position of the maximum wake velocity deficit for each horizontal position. For the ZPG case and for the first turbine in the pressure gradient cases, both normalizations show similar trends. The normalized averaged wake deficit is higher in the APG cases and lower in the FPG cases, compared to the ZPG one behind the first turbine, which is consistent with the previous studies.[25,26] For the in-wake turbine, when normalized by U_h, the APG cases show a lower velocity deficit compared to the FPG ones, whereas when normalized by the base flow velocity along the wake trajectory, it shows a higher value for the APG cases than the FPG ones. In this case, it makes more sense to use the base flow velocity along the wake trajectory as a reference, as it yields trends that are consistent with those for the first turbine wake deficit. It must be noted, however, that for the second turbine, the streamwise pressure gradient is due to the streamwise variation of the wake velocity of the upstream turbine(s), which can be approximated from the evolution of the wake center velocity of the first turbine in the absence of the second one.

To further characterize the wake velocity deficit, we show the evolution of the wake center velocity deficit in Fig. 12. It can be observed that the difference in the wake center velocity deficit between different cases is higher behind the first turbine compared to the second one, no matter what normalization is used. This is an important finding and can be related to the effect of the wake of the first turbine on the second turbine. As all wakes recover with the increase in the downstream distance, they impose a favorable pressure gradient on the downstream turbine(s), which together with the enhanced wake turbulence leads to a faster recovery of the downstream turbine compared to the upstream one.

Figure 13 shows the normalized wake width for different cases. The wake width is obtained by fitting a Gaussian function to the vertical profile of the wake velocity deficit at each downstream distance. Consistent with previous studies Refs. 22, 25, and 26, the wake width behind the first turbine is higher for APG cases and decreases for the ZPG and FPG cases, respectively. In the wake of the second turbine, the same trend holds but the difference between different cases increases compared to that in the first turbine's wake. In addition, the difference is higher between the ZPG and APG cases than that between the ZPG and FPG cases. This is likely due to the fact that the wake moves away from the surface in the APG cases, giving it more space to expand with the streamwise distance, whereas it moves toward the surface in the FPG cases, which limits the expansion of the wake.

Some recent studies have shown that a wind turbine wake follows the base flow streamline originating from the hub position.[26,51] Here, we investigate the trajectory of the cumulative wake of multiple turbines to see if it follows the wake trajectory of the upstream-most turbine or deviates from it. For this purpose, we show the mean wake center trajectory overlaid on the base flow velocity and streamlines in Fig. 14. For majority of the cases, we can see that the wake trajectory for different turbines is approximately aligned with the base flow streamline originating from the hub position of the free flow turbine. One exception is the APG-III case, where for the in-wake turbine, the trajectory is almost horizontal and does not necessarily follow either the upstream turbine or the base flow streamlines. Overall, for most cases, following the base flow streamline from the hub position of the first turbine seems to be a reasonable approximation for the wake

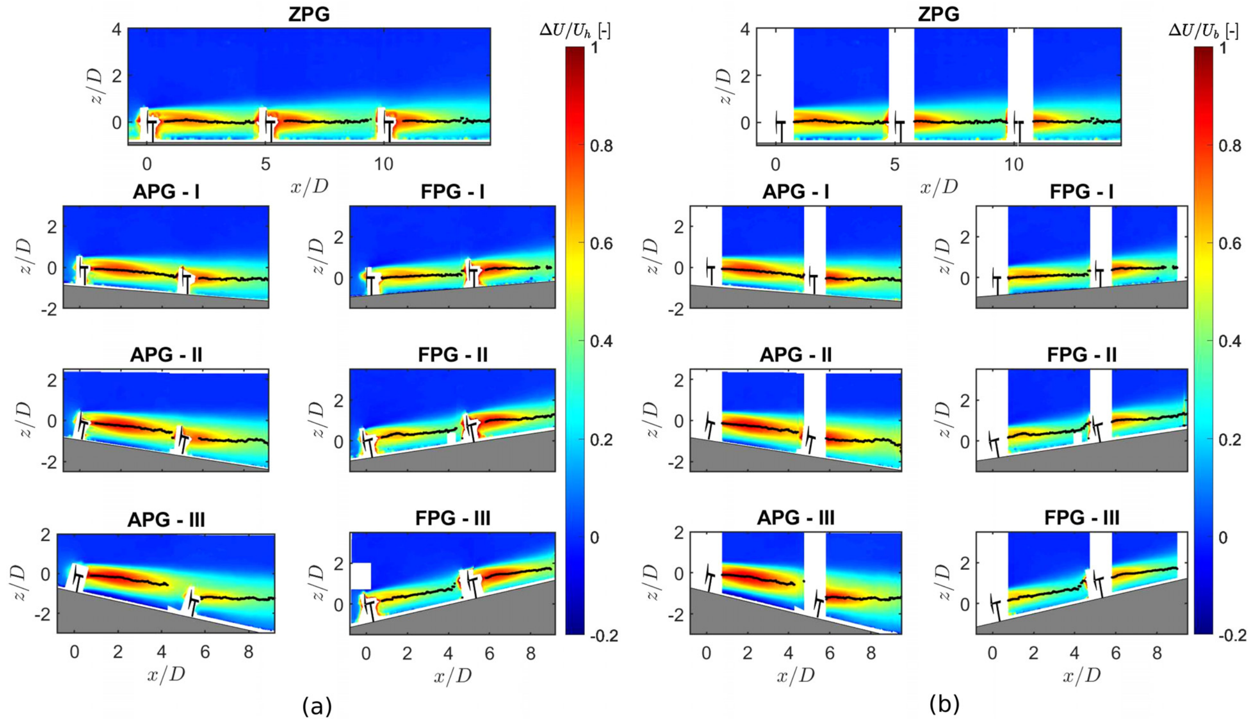

FIG. 11. Contours of the averaged streamwise velocity deficit in the wake flow normalized by the base flow velocity at the hub position of the first turbine (a) and by the base flow velocity along the mean wake trajectory (b) along with the mean wake trajectories (black dots).

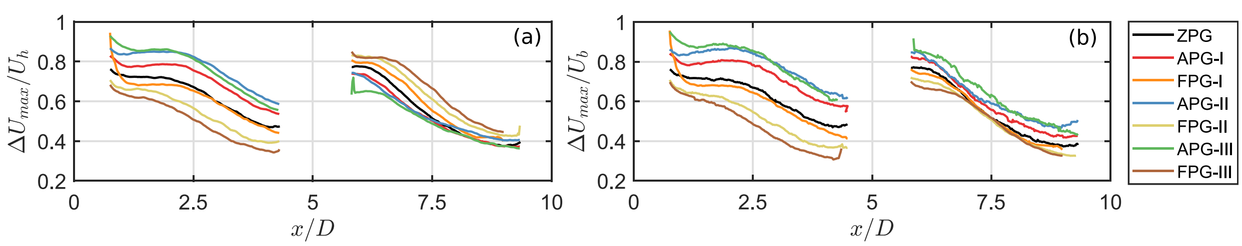

FIG. 12. Wake center velocity deficit normalized by the hub position base flow velocity (a) and by the base flow velocity along the wake center (b).

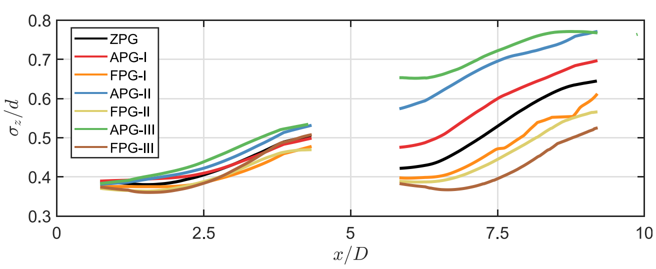

FIG. 13. Comparison of the normalized wake width between different pressure gradient cases.

trajectory of the cumulative wake of multiple turbines under pressure gradient.

III. ANALYTICAL MODELING

In this section, we focus on analytically modeling the cumulative wake velocity deficit of multiple turbines under a pressure gradient. For this purpose, we test two different strategies. The first strategy is based on an adapted version of the linear summation approach proposed by Niayifar and Porté-Agel,[39] whereas the second one is based on the pressure gradient model proposed by Dar and Porté-Agel[26] and Shamsoddin and Porté-Agel.[22] In the following, we will provide details of the two strategies and compare the results obtained from them. For

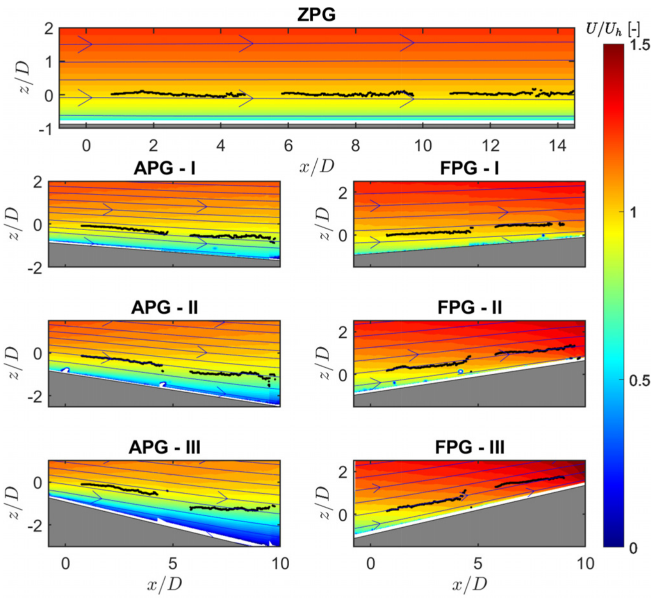

FIG. 14. Contours of the normalized averaged streamwise velocity in the base flow along with the streamlines of the in-plane velocity vectors (arrow lines) and the mean wake trajectories (black dots).

both approaches, the wake velocity deficit in the far wake is assumed to follow a Gaussian distribution given by

$$\frac{U_b - U_w}{U_b} = C(x) e^{-\left(\frac{r^2}{2\sigma(x)^2}\right)}, \tag{1}$$

where U_b is the base flow velocity, U_w is the wake flow velocity, $C(x)$ is the normalized maximum velocity deficit, r is the radial distance from the wake center, and $\sigma(x)$ is the wake width.

A. Adapted linear summation approach

The linear summation approach for the wake superposition proposed by Niayifar and Porté-Agel[39] states

$$U_w(x,y,z) = U_\infty - \sum_i (u_0^i - U_{w,s}^i(x,y,z)), \tag{2}$$

where U_w is the cumulative mean wake velocity, U_∞ is the mean base flow velocity, u_0^i is the mean velocity perceived by the ith turbine, and $U_{w,s}^i$ is the mean wake velocity of the ith wind turbine in stand-alone conditions. In order to adapt the superposition method for a streamwise varying base flow, two changes are made: the base flow velocity U_∞ and the turbine perceived velocity u_0 are expressed as a function of x as $U_b(x)$ and $u_0(x)$, respectively, to account for the variation in the perceived velocity along the wake. The adapted model is then written as

$$U_w(x,y,z) = U_b(x) - \sum_i (u_0^i(x) - U_{w,s}^i(x,y,z)). \tag{3}$$

To model the stand-alone turbine wake, we use the Gaussian model proposed by Bastankhah and Porté-Agel.[30,52] The normalized maximum wake velocity deficit $C(x)$ is modeled as

$$C(x) = 1 - \sqrt{1 - \frac{\sigma_0^2 C_0 (2 - C_0)}{\sigma(x)^2}}. \tag{4}$$

In the above equation, C_0 is the maximum wake velocity deficit at the start of the far wake obtained from the 1D momentum theory ($C_0 = 1 - \sqrt{1 - C_T}$, where $C_T = 0.8$). The start of the far wake is estimated by the near wake length model proposed by Bastankhah and Porté-Agel.[52] The wake width in the far wake σ is assumed to grow linearly with a growth rate k, which is a function of the horizontal turbulence intensity [$k = 0.3TI$ (Ref. 26)]. The wake width at the start of the far wake σ_0 is obtained from experiments. The horizontal turbulence intensity is taken from the base flow information for the free-flow turbine, whereas for the in-wake turbines, the added turbulence intensity of upstream turbines is accounted for, where the total turbulence intensity is then $TI = \sqrt{I_0^2 + I_a^2}$, with I_0 being the base flow turbulence intensity and I_a being the added turbulence intensity. The added turbulence intensity is modeled using the Frandsen model[53]

$$I_a = \frac{1}{1.5 + \frac{0.8}{\sqrt{C_T}} \frac{x}{D}}. \tag{5}$$

B. Pressure gradient model approach

The pressure gradient model proposed initially by Shamsoddin and Porté-Agel[22] and further developed by Dar and Porté-Agel[26,37] accounts for the effect of a base flow streamwise pressure gradient on the evolution of a wind turbine wake. So far, this model has only been applied for stand-alone wind turbine wakes.[12,23,25,46] Here, we look to apply the model for the case of multiple turbines in an aligned condition. The idea behind this is the following: for the first wind turbine, the pressure gradient is solely due to the streamwise variation of the base flow, whereas for the turbines in the wake of upstream ones, the pressure gradient is due to the streamwise variation of the wake flow of the upstream turbines—which already includes the effect of the base flow pressure gradient. In this approach, the effect of the upstream turbine wake(s) is modeled into the base flow term for the downstream turbine wake, which also incorporates the superposition of wakes. In the following, we describe the procedure for applying the model to a multiple turbine case.

The first step is to model the wake of a turbine exposed only to the pressure gradient imposed by the base flow, i.e., the turbine in the no-wake condition. For this purpose, we solve the ordinary differential equation for the maximum velocity deficit

$$\frac{dC}{dx} = \frac{-1}{\left(\frac{U_b^4}{\Lambda_0^2}\right)(3C^2 - 2C^3)} \left[\frac{1}{4} \frac{dU_b^4}{dx} \frac{C^3}{\Lambda_0^2} + \left(C^3 - \frac{C^4}{2} \right) \frac{d}{dx} \left(\frac{U_b^4}{\Lambda_0^2} \right) \right], \tag{6}$$

where U_b is taken as the base flow along the wake trajectory and Λ_0 is the invariant ratio defined as

$$\Lambda_0 = \frac{C_{zpg} U_h}{\sigma_{zpg}}, \tag{7}$$

where U_h is the hub height velocity at the turbine location, C_{zpg} is the maximum velocity deficit under the zero pressure gradient condition, and σ_{zpg} is the wake width under the zero pressure gradient. In order to solve Eq. (6), an estimation of the maximum velocity deficit at the start of the far wake is needed in the form of a boundary condition. This is defined as

$$C_{nw}(x) = 1 - \frac{U_{nw}(x)}{U_b(x)}, \tag{8}$$

where $C_{nw}(x)$ is the normalized maximum velocity deficit in the near wake and U_{nw} is the near wake velocity, which can be obtained as follows:

$$U_{nw}(x) = \sqrt{U_{nb}(x)^2 - U_h^2 C_T}, \tag{9}$$

where U_{nb} is the base flow velocity in the near wake. The estimation of the near wake length is made by solving the following equation:[26]

$$\begin{aligned}\sigma_{nw} = (2\alpha TI + \beta)\int_0^{l_{nw}} \frac{1}{1+\sqrt{1-\frac{U_h^2 C_T}{U_b^2}}}dx \\ - \beta \int_0^{l_{nw}} \frac{1}{1+\frac{1}{\sqrt{1-\frac{U_h^2 C_T}{U_b^2}}}}dx,\end{aligned} \tag{10}$$

where l_{nw} is the near wake length, σ_{nw} is the wake width at the end of the near wake, and α and β are the model constants taken as 0.58 and 0.077, respectively.

Finally, the wake width under pressure gradient can be obtained from the invariant ratio

$$\sigma(x) = \frac{CU_b}{\Lambda_0}. \tag{11}$$

For an in-wake turbine, the wake flow of the upstream turbine(s) becomes the new base flow. In this work, we approximate that base flow from the modeled minimum wake velocity of the upstream turbine and plug it in Eq. (6), where now $U_b = U^{i-1}_{w,\min}$. We also need to estimate the invariant ratio for the in-wake turbine using Eq. (7). Here, U_h is now the wake velocity of the *i-1th* wind turbine at the hub location of the *ith* turbine in its absence. In order to obtain C_{zpg} and σ_{zpg}, we once again need the wake growth rate k, which in this case depends on the base flow turbulence intensity and the wake added turbulence intensity and similar to the linear sum approach can be written as $k = 0.3\sqrt{I_0^2 + I_a^2}$. The added turbulence intensity is estimated using the Frandsen model. The process is repeated in an iterative manner, where for each downstream turbine, the base flow velocity and the invariant ratio are updated based on the cumulative wake velocity of the upstream turbines.

Due to the lack of experimental data for U_w^{i-1} in the overlapping region of $i-1$th and ith turbine wakes, an additional step is needed in order to perform a comparison between the model and the experimental data. This involves re-scaling $C(x)$ and $\sigma(x)$ for the ith turbine with respect to the base flow in the absence of any upstream turbines. The maximum deficit C obtained for the ith turbine can be written as

$$C^i(x) = \left[\frac{U_w^{i-1} - U_w^i}{U_w^{i-1}}\right]_{\max}, \tag{12}$$

which can be used to get the minimum U_w^i and eventually compute the maximum deficit with respect to the base flow without any turbine

$$C(x) = \left[\frac{U_b - U_w^i}{U_b}\right]_{\max}. \tag{13}$$

In order to compute the wake width, the invariant ratio is computed as

$$\Lambda_0^i = \frac{C_{zpg}^i U_{b,x_i}}{\sigma_{zpg}^i}, \tag{14}$$

where U_{b,x_i} is the base flow velocity at the position of the ith turbine. This eventually gives the wake width

$$\sigma(x) = \frac{CU_b}{\Lambda_0^i}. \tag{15}$$

Finally, the wake deficit profiles with respect to the base flow can be computed using Eq. (1). Alternatively, we could use Eq. (1) such that we get U_w^i and then subtract it from the global base flow U_b. Both methods of computing the global wake deficit yield equivalent results.

C. Comparison between experiments and models

We now compare the results from the two modeling approaches described above with the experimental data. Figure 15 compares the normalized maximum velocity deficit in the wake between the experiments and different models. Both approaches yield reasonable results for the ZPG case. By definition, the normalized maximum velocity deficit is the same for all the cases in the linear summation approach, whereas it changes for the pressure gradient model, as it accounts for the effect of the change in the base flow in the computation of the normalized maximum deficit. This is why the result of the pressure gradient model (red line) is observed to change depending on the case, whereas the linear summation (green line) remains the same. For the APG cases, the pressure gradient model is able to predict the normalized maximum velocity deficit well in the far wake of both turbines, whereas the linear summation approach under-predicts it. The under-prediction of the normalized maximum deficit is higher in the wake of the first turbine compared to that in the wake of the second. This is explained by the fact that the difference between the ZPG and the pressure gradient wake deficit is higher in the first turbine wake than in the second turbine one. Similarly, for the FPG cases, the pressure gradient model can predict the normalized maximum velocity deficit well for the FPG-I and FPG-II cases; however, it under-predicts in the FPG-III case. This could be related to the fact that the normalized maximum velocity deficit in the second turbine's wake is comparable between different FPG cases; however, the wake velocity of the first turbine varies. While the experimental data shows a comparable maximum velocity deficit, the one predicted by the model decreases due to the higher FPG of the upstream turbine. As the turbine wake has a downward trajectory into a low momentum region close to the surface with the increase in the ramp angle for FPG cases, this could result in an apparent slowdown of the wake recovery observed in the second turbine wake. It is to be noted that, in the near wake of the turbines, the experimental normalized maximum velocity deficit is higher than the

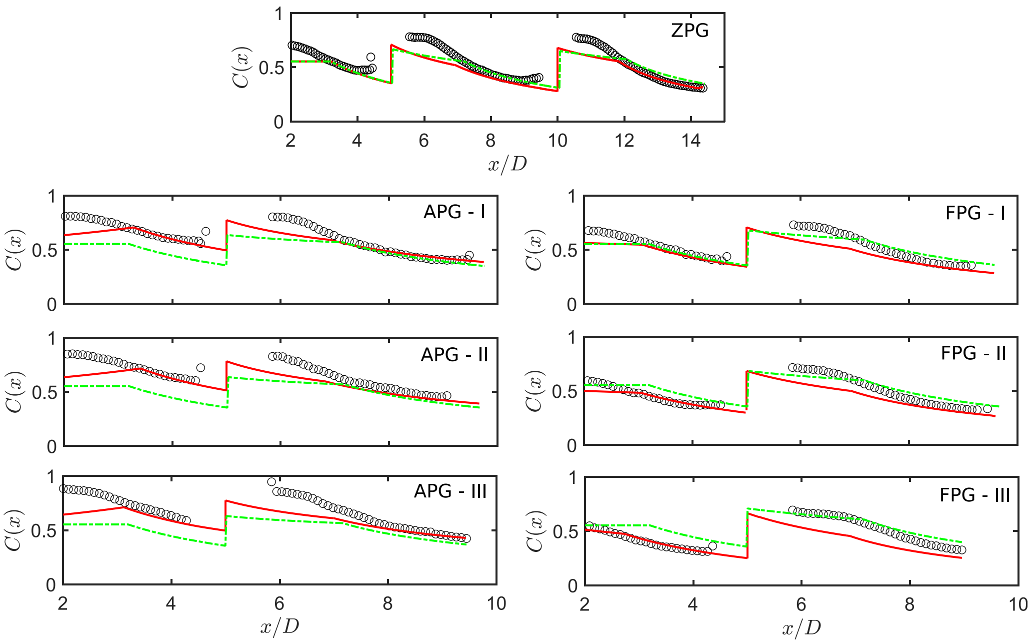

FIG. 15. Comparison of the normalized maximum velocity deficit in the wake between the experiments (circles), the linear superposition approach (green line), and the pressure gradient model (red line).

modeled one. This can be associated with the effects of the turbine hub drag and the rotation of the wake, which are not included in the simplified theoretical estimation of the near wake velocity deficit.[37,42,52] In addition, the Gaussian-based models are applicable in the far wake region and do not conserve momentum in the near wake region. A region of increased normalized maximum velocity deficit can also be observed upstream of the in-wake turbines in the measurements, which is associated with the induction of the turbines. This increase in the normalized maximum velocity deficit in the induction region is most pronounced in the ZPG case and is relatively less significant in the pressure gradient cases. However, this effect is not captured by the analytical wake models. In the future, improved analytical models for the flow in the near wake and induction regions could further enhance the accuracy of the proposed analytical approach.

Figure 16 compares the vertical profiles of the normalized streamwise velocity deficit in the wake for different pressure gradient cases. For the ZPG case, the pressure gradient model is able to predict the velocity deficit profiles behind all three wind turbines with reasonably good accuracy. As a reference, the linear summation approach for wake superposition is also shown to predict the velocity deficit profiles well. This shows that the pressure gradient model can actually be used for predicting the velocity deficit profiles in a wind farm in flat terrain without the need for any subsequent superposition of wakes. For the APG cases, the pressure gradient model predicts the velocity deficit profiles well for all the cases. The linear summation approach, on the other hand, does not yield satisfactory results. Behind the first turbine, there is a significant underestimation of the velocity deficit profiles compared to the experimental data, in terms of both the maximum deficit and the wake width. For the second turbine, the prediction of maximum velocity deficit improves, whereas the wake width is still significantly underestimated compared to the experimental velocity deficit profiles. For the FPG cases, the pressure gradient model agrees reasonably well with the experiments for all cases except the second turbine in the FPG-III case. The linear summation approach results in an overestimation of the maximum velocity deficit for all the cases, except the first turbine in the FPG-I case.

Through this comparison, the pressure gradient model approach to estimate the cumulative wake of multiple turbines in flat and non-flat terrain is validated. The model conserves momentum in the far wake and eliminates the need for any empirical approach to superpose individual wakes. The linear summation approach, on the other hand, does not yield good results for non-flat cases. This can be related to the fact that while it can approximately conserve momentum in the flat case,[42] it cannot account for the pressure gradient imposed by the base flow in non-flat cases.

IV. SUMMARY

Wind turbines in complex terrain can experience pressure gradients due to the change in surface elevation or roughness characteristics. In this study, we systematically investigated the wake of multiple turbines under a range of terrain-induced pressure gradients using wind tunnel experiments. The pressure gradients were imposed by means of linear ramps, where in total, seven different pressure gradient cases were investigated. The flow speed-up/slow-down was linear in all cases, and two turbines were sited on the ramps at an inter-turbine spacing of five rotor diameters, and three turbines were used in the zero pressure gradient case. The focus of the study was to understand the effect of pressure gradient on the cumulative wake of multiple turbines.

The normalized averaged streamwise velocity was shown to decrease behind the in-wake turbine with the increase in the APG compared to that behind the turbine exposed to the free flow. For the

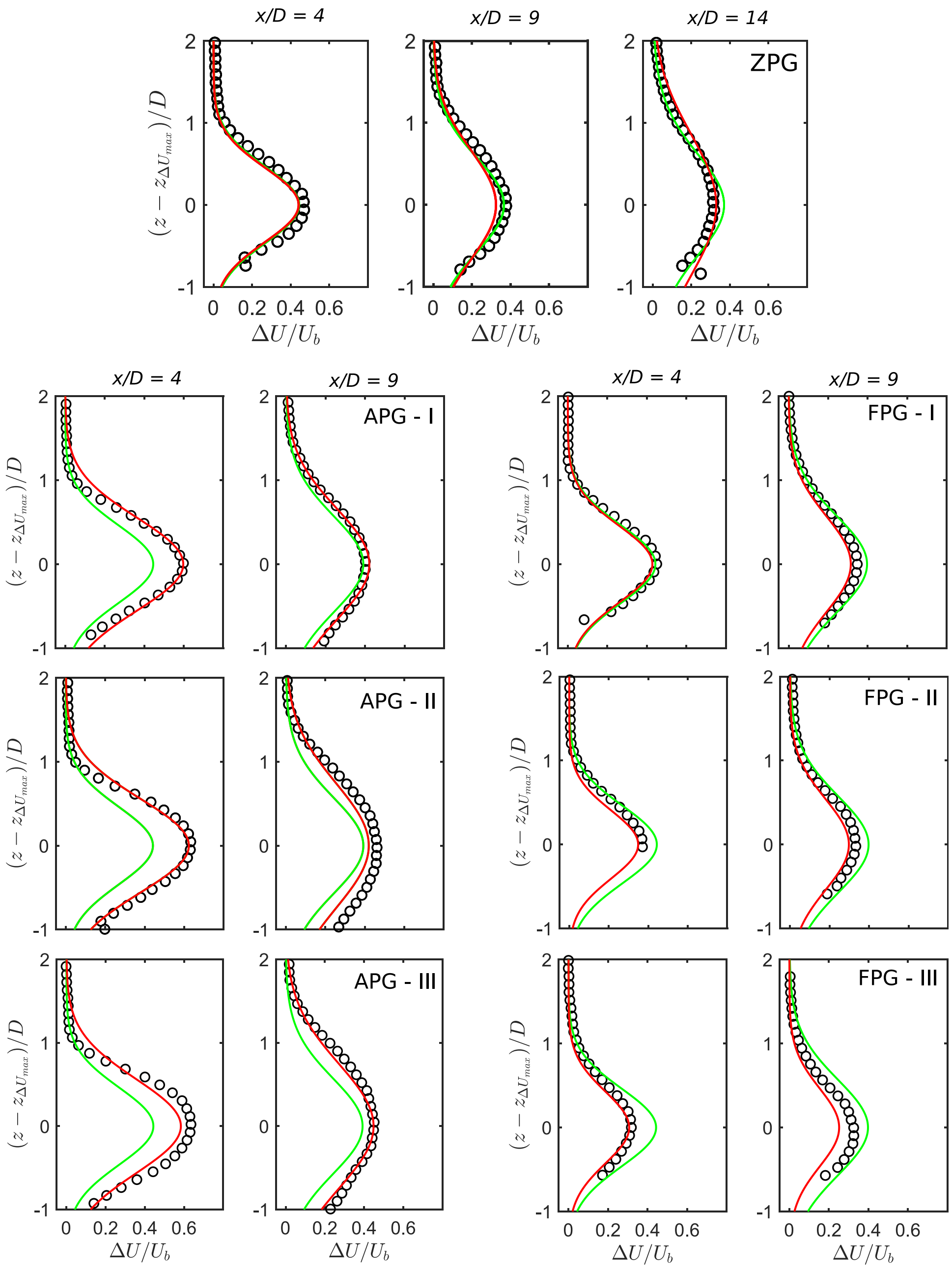

FIG. 16. Comparison of the vertical profiles of the normalized averaged velocity deficit in the wake between the experiments (circles), the linear superposition approach (green line), and the pressure gradient model (red line).

ZPG and FPG cases, on the other hand, the normalized streamwise velocity behind the in-wake turbine increased with an increasing pressure gradient magnitude. This was related to the turbine-added turbulence and the flow speed-up in the FPG cases. The horizontal turbulence intensity showed a peak at the rotor top tip level due to high mean flow shear. The magnitude of the turbulence intensity peak was observed to increase in the cumulative wake of multiple turbines in the ZPG and FPG cases, compared to the upstream-most turbine, whereas no considerable increase in the magnitude was observed for the APG cases. This behavior was associated with the wake trajectory and overlapping of the peak turbulence intensity region of the two turbine wakes. The vertical momentum flux was also observed to change with the ramp slope, which was likely associated with the inclination of the ramp. The vertical momentum flux showed a higher magnitude around the rotor top tip level in APG cases, whereas in the FPG cases, it was stronger near the bottom tip of the turbine.

The wake velocity deficit was also characterized. The velocity deficit behind the first turbine showed a higher difference between different pressure gradient cases than behind the second turbine. This was related to the change in the pressure gradient due to the wake of the upstream turbine. The normalized wake width, on the other hand, showed a higher difference between different cases behind the second turbine than behind the first one. This is likely due to the larger distance traveled by the cumulative wake, leading to a larger cross-stream expansion of the wake.

We proposed a new approach to model the cumulative wake velocity deficit of multiple wind turbines. In this approach, we use the pressure gradient model proposed previously to model stand-alone wind turbine wakes in topography. This is the first instance of the application of the model to a case with multiple wind turbines. To model the wake velocity deficit behind an in-wake turbine, the wake velocity minimum of the upstream turbine(s) wake flow is used as a base flow to estimate the maximum wake velocity deficit, and the invariant ratio is used to obtain the wake width. The new approach is tested against the linear summation approach to superpose the wake velocity deficit of stand-alone turbines and against the experimental data. For the wind farm in flat terrain, both methods of modeling the velocity deficit yield reasonable results. For the two turbine cases under pressure gradient, the new approach is found to agree well with the experiments for most of the cases and outperforms the approach based on the linear summation superposition. Therefore, with the new approach, we can model wind farm wakes in flat and complex terrains without the need for any superposition principle.

ACKNOWLEDGMENTS

This research was funded by the Swiss National Science Foundation (Grant Nos. 200021_172538 and 200021_215288) and the Swiss Federal Office of Energy (Grant No. SI/502135-01).

AUTHOR DECLARATIONS

Conflict of Interest

The authors have no conflicts to disclose.

Author Contributions

Arslan Salim Dar: Conceptualization (equal); Data curation (lead); Formal analysis (lead); Investigation (lead); Methodology (lead); Writing – original draft (lead). **Fernando Porte-Agel:** Conceptualization (equal); Formal analysis (supporting); Funding acquisition (lead); Investigation (supporting); Methodology (supporting); Supervision (lead); Writing – review & editing (lead).

DATA AVAILABILITY

The data will be made available upon reasonable request.

NOMENCLATURE

C	Normalized wake velocity deficit
C_T	Thrust coefficient
C_0	Normalized velocity deficit at the start of the far wake
D	Rotor diameter
h	Ramp height
I_a	Added turbulence intensity
I_U	Streamwise turbulence intensity
I_0	Base flow turbulence intensity
k	Wake growth rate
K	Torque constant
l	near wake length
P	Mean power
Q	Shaft torque
Q_f	Frictional torque
r	Radial distance from the wake center
TI	total turbulence intensity
u_0	Velocity perceived by the in-wake turbine
u_*	Friction velocity
$\overline{u'w'}$	Vertical momentum flux
U	Streamwise velocity
x	Horizontal coordinate
y	Lateral coordinate
z	Vertical coordinate
z_h	Turbine hub height
z_0	Aerodynamic surface roughness
α, β	model constants
ΔU	Streamwise velocity deficit
$\Delta U_{\max}$	Maximum velocity deficit
Λ_0	Invariant ratio
σ	Wake width
σ_U	Standard deviation in U
σ_0	Wake width at the start of the far wake
Ω	Turbine rotational speed

Subscripts

b	Base flow
h	Hub height
nb	base flow in the near wake
nw	near wake
w	Wake flow
x	Horizontal direction
z	Vertical direction
zpg	Zero pressure gradient
∞	Undisturbed flow

REFERENCES

[1]GWEC, "Global wind report 2022," Annual Report (Global Wind Energy Council, 2022).

[2]IRENA, "Renewable power generation costs in 2021," Annual Report (International Renewable Energy Agency, 2022).

[3]F. Porté-Agel, M. Bastankhah, and S. Shamsoddin, "Wind-turbine and wind-farm flows: A review," Boundary-Layer Meteorol. **174**, 1–59 (2020).

[4]R. J. A. M. Stevens and C. Meneveau, "Flow structure and turbulence in wind farms," Annu. Rev. Fluid Mech. **49**, 311–339 (2017).

[5]W. Tian, A. Ozbay, W. Yuan, P. Sarakar, H. Hu, and W. Yuan, "An experimental study on the performances of wind turbines over complex terrain," AIAA Paper No. 2013-0612, 2013.

[6]A. Hyvärinen and A. Segalini, "Effects from complex terrain on wind-turbine performance," J. Energy Resour. Technol. **139**, 051205 (2017).

[7]A. S. Dar and F. Porté-Agel, "Three-dimensional wind-turbine wake characterization via tomographic particle-image velocimetry," J. Phys.: Conf. Ser. **1618**, 062045 (2020).

[8]A. S. Dar and F. Porté-Agel, "Wind turbine wakes on escarpments: A wind-tunnel study," Renewable Energy **181**, 1258–1275 (2022).

[9]E. S. Politis, J. Prospathopoulos, D. Cabezon, K. S. Hansen, P. K. Chaviaropoulos, and R. J. Barthelmie, "Modeling wake effects in large wind

farms in complex terrain: The problem, the methods and the issues," Wind Energy **15**, 161–182 (2012).

[10]A. S. Dar, J. Berg, N. Troldborg, and E. G. Patton, "On the self-similarity of wind turbine wakes in a complex terrain using large eddy simulation," Wind Energy Sci. **4**, 633–644 (2019).

[11]L. Liu and R. J. A. M. Stevens, "Effects of two-dimensional steep hills on the performance of wind turbines and wind farms," Boundary-Layer Meteorol. **176**, 251–269 (2020).

[12]Z. Zhang, P. Huang, G. Bitsuamlak, and S. Cao, "Large-eddy simulation of wind-turbine wakes over two-dimensional hills," Phys. Fluids **34**, 065123 (2022).

[13]N. Troldborg, S. J. Andersen, E. L. Hodgson, and A. Meyer Forsting, "Brief communication: How does complex terrain change the power curve of a wind turbine?" Wind Energy Sci. **7**, 1527–1532 (2022).

[14]R. Menke, N. Vasiljević, K. S. Hansen, A. N. Hahmann, and J. Mann, "Does the wind turbine wake follow the topography? A multi-lidar study in complex terrain," Wind Energy Sci. **3**, 681–691 (2018).

[15]X. Han, D. Liu, C. Xu, and W. Z. Shen, "Atmospheric stability and topography effects on wind turbine performance and wake properties in complex terrain," Renewable Energy **126**, 640–651 (2018).

[16]W. C. Radünz, Y. Sakagami, R. Haas, A. P. Petry, J. C. Passos, M. Miqueletti, and E. Dias, "Influence of atmospheric stability on wind farm performance in complex terrain," Appl. Energy **282**, 116149 (2021).

[17]P. G. Hill, U. Schaub, and Y. Senoo, "Turbulent wakes in pressure gradients," J. Appl. Mech. **30**, 518–524 (1963).

[18]X. Liu, F. O. Thomas, and R. C. Nelson, "An experimental investigation of the planar turbulent wake in constant pressure gradient," Phys. Fluids **14**, 2817–2838 (2002).

[19]F. O. Thomas and X. Liu, "An experimental investigation of symmetric and asymmetric turbulent wake development in pressure gradient," Phys. Fluids **16**, 1725–1745 (2004).

[20]M. M. Rogers, "The evolution of strained turbulent plane wakes," J. Fluid Mech. **463**, 53–120 (2002).

[21]S. Shamsoddin and F. Porté-Agel, "Turbulent planar wakes under pressure gradient conditions," J. Fluid Mech. **830**, R4 (2017).

[22]S. Shamsoddin and F. Porté-Agel, "A model for the effect of pressure gradient on turbulent axisymmetric wakes," J. Fluid Mech. **837**, R3 (2018).

[23]S. Shamsoddin and F. Porté-Agel, "Wind turbine wakes over hills," J. Fluid Mech. **855**, 671–702 (2018).

[24]J. Hunt, S. Leibovich, and K. Richards, "Turbulent shear flows over low hills," Q. J. R. Meteorol. Soc. **114**, 1435–1470 (1988).

[25]T. Cai, S. Cheng, A. Segalini, and L. P. Chamorro, "Local topography-induced pressure gradient effects on the wake and power output of a model wind turbine," Theor. Appl. Mech. Lett. **11**, 100297 (2021).

[26]A. S. Dar, A. S. Gertler, and F. Porté-Agel, "An experimental and analytical study of wind turbine wakes under pressure gradient," Phys. Fluids **35**, 045140 (2023).

[27]D. Siguenza-Alvarado, V. Pulletikurthi, J. J. Quinones, C. Nelson, S. Cheng, A. Doosttalab, L. P. Chamorro, and L. Castillo, "Wake interaction of aligned wind turbines over two-dimensional hills," Phys. Fluids **35**, 105142 (2023).

[28]N. O. Jensen, "A note on wind gnerator interaction," Report No. Risø-M-2411, Risø National Laboratory, Roskilde, Denmark, 1983.

[29]S. Frandsen, R. Barthelmie, S. Pryor, O. Rathmann, S. Larsen, J. Højstrup, and M. Thøgersen, "Analytical modelling of wind speed deficit in large offshore wind farms," Wind Energy **9**, 39–53 (2006).

[30]M. Bastankhah and F. Porté-Agel, "A new analytical model for wind-turbine wakes," Renewable Energy **70**, 116–123 (2014).

[31]T. Ishihara and G.-W. Qian, "A new Gaussian-based analytical wake model for wind turbines considering ambient turbulence intensities and thrust coefficient effects," J. Wind Eng. Ind. Aerodyn. **177**, 275–292 (2018).

[32]M. Abkar, J. N. Sørensen, and F. Porté-Agel, "An analytical model for the effect of vertical wind veer on wind turbine wakes," Energies **11**, 1838 (2018).

[33]N. Bempedelis and K. Steiros, "Analytical all-induction state model for wind turbine wakes," Phys. Rev. Fluids **7**, 034605 (2022).

[34]D. Vahidi and F. Porté-Agel, "A physics-based model for wind turbine wake expansion in the atmospheric boundary layer," J. Fluid Mech. **943**, A49 (2022).

[35]H. Sun, X. Gao, and H. Yang, "Validations of three-dimensional wake models with the wind field measurements in complex terrain," Energy **189**, 116213 (2019).

[36]R. Brogna, J. Feng, J. N. Sørensen, W. Z. Shen, and F. Porté-Agel, "A new wake model and comparison of eight algorithms for layout optimization of wind farms in complex terrain," Appl. Energy **259**, 114189 (2020).

[37]A. S. Dar and F. Porté-Agel, "An analytical model for wind turbine wakes under pressure gradient," Energies **15**, 5345 (2022).

[38]P. Lissaman, "Energy effectiveness of arbitrary arrays of wind turbines," J. Energy **3**, 323–328 (1979).

[39]A. Niayifar and F. Porté-Agel, "Analytical modeling of wind farms: A new approach for power prediction," Energies **9**, 741 (2016).

[40]I. Katic, J. Højstrup, and N. O. Jensen, "A simple model for cluster efficiency," in *European Wind Energy Association Conference and Exhibition* (A. Raguzzi Rome, Italy, 1986), Vol. 1, pp. 407–410.

[41]S. Voutsinas, K. Rados, and A. Zervos, "On the analysis of wake effects in wind parks," Wind Eng. **14**, 204–219 (1990).

[42]H. Zong and F. Porté-Agel, "A momentum-conserving wake superposition method for wind farm power prediction," J. Fluid Mech. **889**, A8 (2020).

[43]M. Bastankhah, B. L. Welch, L. A. Martínez-Tossas, J. King, and P. Fleming, "Analytical solution for the cumulative wake of wind turbines in wind farms," J. Fluid Mech. **911**, A53 (2021).

[44]L. Lanzilao and J. Meyers, "A new wake-merging method for wind-farm power prediction in the presence of heterogeneous background velocity fields," Wind Energy **25**, 237–259 (2022).

[45]M. Bastankhah and F. Porté-Agel, "A new miniature wind turbine for wind tunnel experiments. Part I: Design and performance," Energies **10**, 908 (2017).

[46]A. S. Dar, G. Armengol Barcos, and F. Porté-Agel, "An experimental investigation of a roof-mounted horizontal-axis wind turbine in an idealized urban environment," Renewable Energy **193**, 1049–1061 (2022).

[47]B. Wieneke, "PIV uncertainty quantification from correlation statistics," Meas. Sci. Technol. **26**, 074002 (2015).

[48]L. P. Chamorro, R. E. Arndt, and F. Sotiropoulos, "Reynolds number dependence of turbulence statistics in the wake of wind turbines," Wind Energy **15**, 733–742 (2012).

[49]R. Deshpande and I. Marusic, "Characterising momentum flux events in high Reynolds number turbulent boundary layers," Fluids **6**, 168 (2021).

[50]Y.-T. Wu and F. Porté-Agel, "Atmospheric turbulence effects on wind-turbine wakes: An LES study," Energies **5**, 5340–5362 (2012).

[51]Z. Liu, S. Lu, and T. Ishihara, "Large eddy simulations of wind turbine wakes in typical complex topographies," Wind Energy **24**, 857–886 (2021).

[52]M. Bastankhah and F. Porté-Agel, "Experimental and theoretical study of wind turbine wakes in yawed conditions," J. Fluid Mech. **806**, 506–541 (2016).

[53]S. Frandsen, "Turbulence and turbulence-generated structural loading in wind turbine clusters," Risoe-R No. 1188(EN), 2007.